Precipitation Distribution in Tropical Cyclones Using the Tropical Rainfall Measuring Mission (TRMM) Microwave Imager: A Global Perspective

MANUEL LONFAT

Rosenstiel School of Marine and Atmospheric Science, University of Miami, Miami, Florida

FRANK D. MARKS, JR.

Hurricane Research Division, NOAA/AOML, Miami, Florida

SHUYI S. CHEN

Rosenstiel School of Marine and Atmosphere Science, University of Miami, Miami, Florida

(Manuscript received 16 July 2003, in final form 21 December 2003)

ABSTRACT

TRMM microwave imager rain estimates are used to quantify the spatial distribution of rainfall in tropical cyclones (TCs) over the global oceans. A total of 260 TCs were observed worldwide from 1 January 1998–31 December 2000, providing 2121 instantaneous TC precipitation observations. To examine the relationship between the storm intensity, its geographical location, and the rainfall distribution, the dataset is stratified into three intensity groups and six oceanic basins. The three intensity classes used in this study are tropical storms (TSs) with winds <33 m s^{-1}, category 1–2 hurricane-strength systems (CAT12) with winds from 34–48 m s^{-1}, and category 3–5 systems (CAT35) with winds >49 m s^{-1}. The axisymmetric component of the TC rainfall is represented by the radial distribution of the azimuthal mean rainfall rates (R). The mean rainfall distribution is computed using 10-km annuli from the storm center to a 500-km radius. The azimuthal mean rain rates vary with storm intensity and from basin to basin. The maximum R is about 12 mm h^{-1} for CAT35, but decreases to 7 mm h^{-1} for CAT12, and to 3 mm h^{-1} for TS. The radius from the storm center of the maximum rainfall decreases with increasing storm intensity, from 50 km for TS to 35 km for CAT35 systems. The asymmetric component is determined by the first-order Fourier decomposition in a coordinate system relative to the storm motion. The asymmetry in TC rainfall varies significantly with both storm intensity and geographic locations. For the global average of all TCs, the maximum rainfall is located in the front quadrants. The location of the maximum rainfall shifts from the front-left quadrant for TS to the front-right for CAT35. The amplitude of the asymmetry varies with intensity as well; TS shows a larger asymmetry than CAT12 and CAT35. These global TC rainfall distributions and variability observed in various ocean basins should help to improve TC rainfall forecasting worldwide.

1. Introduction

Predicting rainfall associated with tropical cyclones (TCs) is a major operational challenge. Over the last few decades, freshwater flooding has become the largest threat to human lives from TCs at landfall in the United States (Rappaport 2000). While track forecasts continue to improve, quantitative precipitation forecasts (QPF) for TCs have shown little skill. One of the uncertainties in QPF is a lack of precipitation data over the open oceans to evaluate and validate numerical weather prediction (NWP) model results. Early empirical TC rainfall forecast models assume either a constant rain rate or axisymmetric rainfall distribution in TCs. A number of case studies have shown that the precipitation structures in TCs are quite complex and vary from case to case (e.g., Miller 1958; Frank 1977; Marks 1985; Burpee and Black 1989). This study will provide a comprehensive analysis of the global TC rainfall characteristics using the Tropical Rainfall Measuring Mission (TRMM) observations. It is a critical step toward understanding and improving QPF in TCs.

Early radar images revealed that the TC rainfall is usually organized in bands spiraling toward the storm center (Wexler 1947), commonly referred to as rainbands. A ring of intense rainfall surrounds the storm center (e.g., Kessler 1958; Jordan et al. 1960), known as the eyewall. The spatial distribution of TC rainfall can be thought of as a series of annular means composed of an azimuthal mean (or axisymmetric) and a pertur-

Corresponding author address: Dr. Shuyi S. Chen, RSMAS/University of Miami, Miami, FL 33149.
E-mail: schen@rsmas.miami.edu

bation (or asymmetric) component. Miller (1958) made a composite of rain gauge data from 16 hurricanes over Florida in a 3° array aligned with the TC track. He observed a mean rain rate of 6.6 mm h^{-1} in the 1° box directly surrounding the storm center. The mean rain rate in the remaining outer domain was 3.2 mm h^{-1}. Rodgers and Adler (1981) constructed radial profiles of rainfall for 21 eastern and western Pacific cyclones using satellite passive microwave imager observations. They found that TC intensification was accompanied not only by increases in the average rain rate, but also in the relative contribution of the heavy rainfall. They also found that the radius of maximum rainfall decreased with increasing storm intensity. Using airborne radar measurements Marks (1985) found an azimuthal mean rain rate of 11 mm h^{-1} in the eyewall of Hurricane Allen (1980), which was about 6 times of that from the eyewall to a 111-km radius. Burpee and Black (1989) examined the radar-derived rainfall structure within 75 km of the center of Hurricanes Alicia (1983) and Elena (1985). They found that the azimuthal mean rain rates in the eyewall were only 5.2 and 6 mm h^{-1}, respectively. The rates dropped to 2.8 and 3.4 mm h^{-1} in the first rainband around the storm center. These studies also showed that each storm has very different rainfall distributions during its evolution, suggesting that many factors, both related to the storm dynamics and to its environment, can influence the rainfall structure.

Asymmetries in the TC rainfall have been studied both observationally and numerically. Radar observations showed rainfall asymmetry in Hurricanes Allen (Marks 1985), Alicia, and Elena (Burpee and Black 1989). However, the asymmetry varied significantly from storm to storm. Hurricane Allen had a rain-rate maximum in the front-right quadrant in the eyewall region that shifted anticyclonically in the outer region. The rainfall maximum in Hurricane Alicia was first observed in the front-left quadrant and later changed to the front-right quadrant. Other observations have showed mixed results. Miller (1958) showed a maximum rainfall in the front-right quadrant from the 16-storm composite for Florida. Frank (1977) found that rainfall distributions were mainly axisymmetric for western North Pacific storms, using a 21-yr record of rain gauges on 13 small islands. Using satellite observations, Rodgers et al. (1994) showed a front maximum in a North Atlantic TC composite. The location of the maximum shifted to the front-right as the storm translation speed increases. Although most previous studies found a precipitation maximum ahead of the storm center, the variability in the location and amplitude was large. In fact, storms with very similar locations, intensity, and speed, such as Hurricanes Allen, Alicia, and Elena, can have very different rainfall structures.

The TC rainfall distribution is determined by many factors, including, but not limited to, environmental factors such as wind shear, sea surface temperatures (SST), and moisture distribution, as well as TC-specific factors such as intensity, location, and translation speed. To examine how these factors affect the TC rainfall, a quantitative description of the rain variability is needed as a function of radius and azimuth around the storm center for various TC intensities, locations, and translation speeds.

In this study, the TRMM Microwave Imager rainfall product from 1998 to 2000 is used to determine TC rainfall distributions over the global tropical oceans. Rainfall distributions for the whole database separated by radius and azimuth for various TC intensity, location, and speed are discussed.

2. Data and analysis method

a. TRMM data

TRMM is a joint mission between the U.S. National Aeronautics and Space Administration (NASA) and the Japanese National Space Development Agency (NASDA). The goal of TRMM is to measure global tropical rainfall (Simpson et al. 1988). The main instruments onboard TRMM are a microwave imager (TMI), precipitation radar (PR), and a visible and infrared radiometer system (VIRS). The TRMM satellite was launched in November 1997. Before August 2001, it orbited at a 35° inclination and an altitude of 350 km. The satellite altitude was then increased to 402 km to extend the mission lifetime. The potential of the satellite resides in its ability to access both passive and active radiometric information. The 35° inclination and TRMM's non-sun-synchronous orbit makes it an ideal platform to study TCs. Details of TRMM instruments are given in Kummerow et al. (1998).

The TMI surface rainfall estimates (Kummerow et al. 1996) are used in this study. The TMI swath is 750 km wide and the footprint is an ellipse with nearly 4- and 6-km axes. The TRMM orbits containing TCs are selected by matching the TRMM database to linearly interpolated best track information globally. The interpolated data provide the TC location, intensity, speed, and direction of motion every 10 s. The times are matched to those for the TRMM orbits and the distance between the storm center and the TRMM satellite nadir is computed. If the distance is smaller than 500 km, the satellite observation is used in the analysis. A maximum radius of 500 km was used to ensure the data coverage exceeded 20% of the total area for all radii. As will be illustrated later, the data coverage decreases rapidly beyond 500-km radius. Only observations over the ocean are considered as the TMI rain algorithm underestimates light rain over land.

b. TMI global sampling

During the period of 1 January 1998–31 December 2000, 260 TCs were observed globally, providing 2121 TMI instantaneous observations (Fig. 1). In this study,

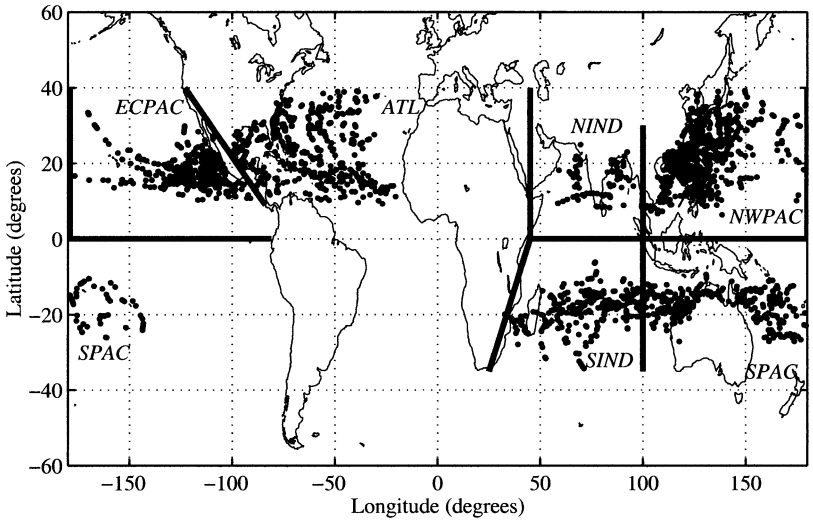

FIG. 1. Tropical cyclones observed by TMI during the period from 1 Jan 1998 to 31 Dec 2000. Each dot represents one TRMM observation. The solid lines indicate the boundaries of the six active oceanic basins.

tropical storms (TSs) are defined as systems with wind speed[1] from 18 to 33 m s^{-1}, category 1–2 (CAT12) systems with wind between 34 and 48 m s^{-1}, and category 3–5 (CAT35) systems with wind >49 m s^{-1}. The database contains observations from tropical storm to category 5 hurricane intensity. Approximately 64% (1361) of the 2121 events are TS, 26% (548) are CAT12, and 10% (212) are CAT35 systems.

The observations are distributed among all TC basins around the globe. Six basins are considered: Atlantic (ATL), east-central Pacific (ECPAC), northwest Pacific (NWPAC), north Indian Ocean (NIND), south Indian Ocean (SIND), and South Pacific (SPAC). The boundaries between basins are shown in Fig. 1. In order to determine if the TRMM dataset is representative of the distribution of TCs over the 3-yr period, the global TC distribution observed by TRMM was compared to the best track record. Table 1 shows the percentage of all observations and the best track information in each intensity and basin group.

The best track and TRMM distributions are similar for most categories in Table 1. The TRMM dataset is slightly biased toward strong storms in the Atlantic, as 50% of TRMM observations are for hurricanes compared to 45.5% of the best track records. The combined TRMM and the best track CAT12 and CAT35 frequencies are much higher in ATL than the global average during the 1998–2000 period. All other basins, except NIND, show a combined CAT12 and CAT35 percentage below the global average. The large number of CAT12 and CAT35 observations in the Atlantic can be explained by the cold phase of ENSO for the period sampled, during which more intense storms are expected in the Atlantic (Gray 1984; Shapiro 1987). During 1998, ENSO shifted from a cold to a neutral phase in which it remained through the sampled period. NIND shows the largest discrepancy between the satellite database and the best track distribution, as 36% of all NIND TRMM observations correspond to hurricanes, while the best track states that only 26% were for CAT12 or higher. Finally, TRMM's sampling of the NWPAC is

[1] The 6-h best track peak surface wind speeds interpolated to the TRMM orbit time are used to determine the storm intensity. In most basins, the peak wind speed is estimated from the 10-min mean wind, whereas in the ECPAC and ATL basins it is the 1-min sustained wind.

TABLE 1. Comparison of TRMM TC observations and 6-hourly advisory distributions with the cyclone intensity, in each oceanic basin. Percent of total for basin in parentheses.

	TS		CAT12		CAT35		Total	
Basin	TRMM	Best track	TRMM	Best track	TRMM	Best track	TRMM	Best track
ATL	238 (50)	651 (54.5)	178 (37.5)	385 (32)	60 (12.5)	162 (13.5)	476 (22.5)	1198 (21.5)
ECPAC	234 (69)	880 (68)	74 (22)	280 (22)	31 (9)	132 (10)	339 (16)	1292 (23)
NWPAC	455 (67.5)	1128 (71)	168 (25)	331 (21)	52 (7.5)	124 (8)	675 (32)	1583 (28)
NIND	46 (64)	177 (74)	17 (23.5)	40 (16.5)	9 (12.5)	23 (9.5)	72 (3.5)	240 (4.5)
SIND	168 (70)	329 (75.5)	50 (21)	69 (16)	21 (9)	37 (8.5)	239 (11)	435 (7.5)
SPAC	220 (69)	609 (69.5)	61 (19)	174 (20)	39 (12)	94 (10.5)	320 (15)	877 (15.5)
Total	1361 (64)	3774 (67)	548 (26)	1279 (23)	212 (10)	572 (10)	2121	5625

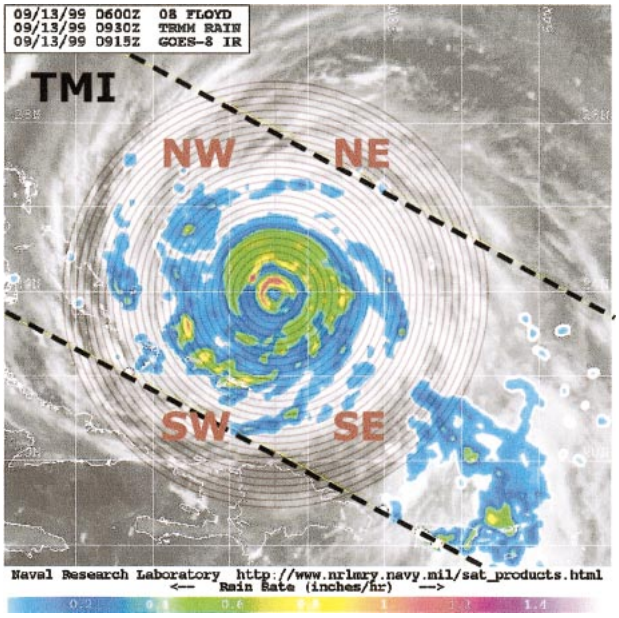

FIG. 2. Example of annuli used in the analysis. The map shows the surface rainfall for Hurricane Floyd on 13 Sep 1999.

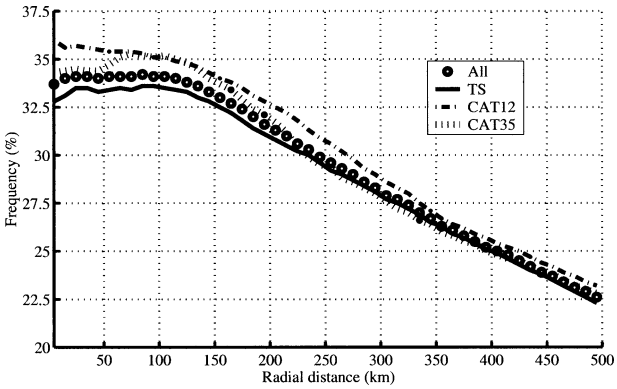

FIG. 3. TRMM/TMI TC data coverage as a function of distance from the TC center, computed relative to the max possible coverage. The max possible coverage for one 10-km-wide annulus around the TC center is defined as the number of TRMM overpasses multiplied by the area within the annulus.

biased toward high TC intensity, compared to the 3-yr best track record average by 3.5%. In summary, the TRMM/TMI dataset is representative of the global TC activity from 1998 to 2000. The rainfall structure that will be discussed later should represent the global TC rainfall well during a rather cold phase of ENSO.

c. Analysis methods

The rainfall characteristics are derived in storm-relative coordinates. The radial variation of precipitation is depicted by the azimuthal mean rain rate in 10-km-wide annuli around the storm center outward to the 500-km radius (Fig. 2). The resulting database allows us to compute the radial dependence of the rain characteristics as a function of the storm intensity, location, and speed.

Most instantaneous observations capture only part of the storm, because 1) the passive microwave swath width is smaller than the size of most storms, and 2) the storm eye and satellite nadir are rarely superimposed. Figure 3 shows the data coverage as a function of radial distance from the TC center, normalized to the maximum possible coverage at all radial distances. The coverage distribution in Fig. 3 is obtained by summing the area for each rain estimate ($\sim$25 km^2) in 10-km annuli around the TC center. These values are then compared to the area of each annulus multiplied by the number of storm events observed by the satellite. For example, for all 2121 events, 8982 rain estimates of the inner 10-km annulus were obtained. The accumulated area for those estimates is 2.3×10^5 km^2. The area of the inner 10-km ring is 314 km^2, yielding a maximum possible coverage of 6.7×10^5 km^2 for the 2121 overpasses. Hence, the ratio between the actual and the ideal coverage is 33.7%. As seen in Fig. 3, the coverage is maintained between 30%–35% out to 200 km, and decreases linearly with radius beyond 200 km. At radii $>$500 km, the coverage decreases sharply below 20% and is therefore not considered in the analysis. Figure 3 also shows that similar results are obtained for the intensity subsets.

The conditional (only when raining) probability density functions (PDFs) of rain-rate occurrence (area) with radial distance can also be determined using the annular database. The PDF is constructed by classifying the TMI rain estimates, for each annulus, in a dBR scale, where

$$\mathrm{dB}R = 10\ \mathrm{Log}_{10}(R). \quad (1)$$

The PDF is constructed for each annulus within the 500-km radius by summing the occurrence of rain estimates in each dBR class. Using the annular PDFs, a contoured frequency by radial distance (CFRD) diagram can be constructed as a function of storm intensity, location, and speed. PDFs and CFRDs provide information on the radial variability of the precipitation distribution, and help to identify the median and mode of the rain-rate distribution at any distance from the center.

To examine the contribution to the total precipitation from various rain rates, PDFs and CFRDs are also constructed for the total precipitation amount in each dBR class. The PDF is obtained by weighing each rain estimate by the corresponding rain rate. The resulting distribution is then normalized to the total amount of rain. This approach provides a PDF distribution normalized by the total rain amount (flux) rather than by the total rain area. The integral over the rain amount PDF divided by the integral over the occurrence PDF is the mean rain rate of the raining area within the annulus. A median and a mode can also be defined for each PDF of rainfall flux, yielding five measures of the rain distribution for each annulus. The mean, median, and mode calculations

TABLE 2. Comparison of TRMM rainfall PDFs with previous studies. The rainfall is partitioned into rate intervals (bins) used in previous studies.

	Rain threshold (mm h^{-1})				
Study	<0.25	0.25–6.25	6.25–19	>19	
Miller (1958) 1° box	32	47	17	4	
Frank (1977) 2° box	30	54	13	3	
Marks (1985) 11 1-km radius	23	69	6	2	
TRMM 111-km radius	0.5	74	21	4.5	
TRMM 222-km radius	1	81	16	2	
TRMM 500-km radius	1	84	13	2	
	Rain threshold (mm h^{-1})				
Study	<2.5	2.5–5	5–10	10–25	>25
Burpee and Black (1989) eyewall, Alicia	59	13	12	12	4
Burpee and Black (1989) eyewall, Elena	58	13	12	11	6
TRMM CAT12 eyewall	34	24	24	14	4

in each PDF can yield very different values, particularly when the PDF distribution is skewed. For TCs, the mode of the distribution is expected to shift toward smaller rain rates as the distance from the center increases.

The next step of our analysis consists in studying the first-order asymmetry of the rain distribution. The asymmetry is defined relative to the storm motion. The direction of the storm motion at each TRMM observation is determined by linear interpolation of the two closest best track reports to the observation time. As for the mean R computations, 10-km-wide annuli around the TC center are used to compute the spatial rainfall asymmetry. It is important to note that missing data in the best track reduce the number of TRMM observations available for the analysis. Nearly 80% of the initial TRMM observations can be assigned a storm direction.

In each annulus, the first-order Fourier coefficients are computed using all rain estimates (Boyd 2001):

$$a_1 = \sum_i [R_i \cos(\theta_i)], \quad (2)$$

$$b_1 = \sum_i [R_i \sin(\theta_i)], \quad (3)$$

where R_i is each individual rain estimate and θ_i the phase angle of the estimate relative to the storm motion. The spatial structure of the first-order asymmetry (M_1) can be represented by

$$M_1 = [a_1 \cos(\theta) + b_1 \sin(\theta)]/R, \quad (4)$$

where R is the mean rain rate calculated over the entire annulus. The first-order asymmetry is computed for different storm intensities, speeds, and locations.

d. Comparison of TMI estimates with other datasets

The previous studies (e.g., Miller 1958; Frank 1977; Marks 1985; Burpee and Black 1989) that discussed the frequency distribution of rainfall in TCs can be used to estimate the quality of the TMI rainfall observations. Table 2 shows the rain-rate stratifications previous authors have used to construct the PDF. Examination of Table 2 shows that the TRMM frequency distributions are similar to those from previous studies, both for the total storm PDF and for the eyewall PDF. Rates <0.25 mm h^{-1} are much less frequent in the TRMM PDF, and rates between 0.25 and 6.25 mm h^{-1} occur more often. Consequently, TRMM redistributes very low rates among the surrounding rainfall bins. As a result, the mean distributions will not be affected except in the area where many 1–2.5 mm h^{-1} rates are observed. However, it likely will not impact the mean rainfall, because nonraining areas weigh heavily in the mean R calculation. TMI estimates become particularly powerful in the asymmetry analysis, which is a normalized calculation with accuracy strongly depending on the size of the dataset.

The differences between TMI and other instruments may also illustrate the difficulties in comparing PDFs of instruments with a wide range of resolutions. Miller (1958) and Frank (1977) results are based on rain gauge networks. Their datasets were large, but gauges only offer point measurements with 1-h accumulation and sampling area ($\sim 10^3$ m^2) three orders of magnitude smaller than that for TMI ($\sim$25 km^2). The comparisons with the PDF of radar estimates are better than those from the gauges. Typical sampling area of ground and airborne radars are around 16 km^2, which is closer to the TMI sampling area.

3. Hurricane Dennis (1999)

The analysis methods described in section 2 are illustrated using a TRMM observation of Hurricane Dennis on 29 August 1999. At 1800 UTC on 29 August, Dennis was off the coast of northeastern Florida, at approximately 30.8°N and 78.4°W. The minimum sea level pressure (MSLP) was near 970 hPa and the maximum sustained winds were about 50 m s^{-1}, making Dennis a category 3 hurricane. Dennis was moving almost due north at 5 m s^{-1}. Dennis's rainfall displayed strong azimuthal variability in rainfall rates (Fig. 4). The rain was mostly on the left and front-left of the storm

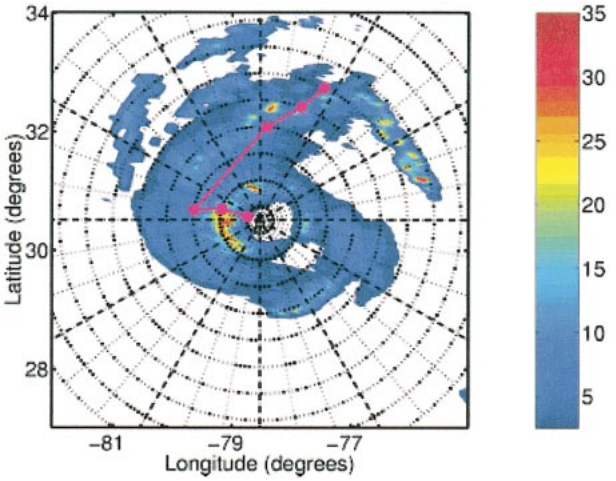

FIG. 4. TMI surface rainfall (in mm h^{-1}) of Hurricane Dennis, on 28 Aug 1999. The dots indicate the location of the phase max of the rainfall asymmetry as a function of the distance to the storm center. The circles (broken lines) are drawn at 50-km radial increments.

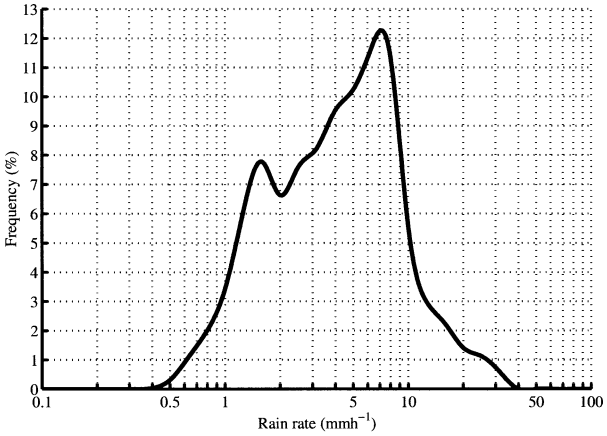

FIG. 6. PDF of rainfall for Dennis within 300-km radius of the storm center.

center in the inner 150 km. In the outer region, the rainfall was mainly located in a strong rainband on the front and front-right of the storm center.

Figure 5 shows the unconditional azimuthal mean rain rates as a function of the radial distance from the storm center in Hurricane Dennis. The peak rainfall is located 60 km from the center and is about 13.5 mm h^{-1}. Several secondary peaks in rainfall can be seen at 150- and 275-km radii, corresponding to a broad zone of precipitation in the front-left quadrant of the storm, and a more intense but narrower region farther to the front-right quadrant of the storm (Fig. 4). The eyewall is well defined in the precipitation distribution, at 60 km from the center. The eye is not totally clear of rain.

The PDF of rain occurrence for the entire storm is shown in Fig. 6. Rain rates are between 0.4 and 40 mm h^{-1}. Most of the rainfall area (~91%) within 500 km of Dennis's center falls between 1 and 10 mm h^{-1}. It is important to note that rainfall covers only 25% of the total area within 500 km of the storm center. The mode is at 7 mm h^{-1}. The distribution also shows a secondary maximum near 1.5 mm h^{-1}. The stratiform rain area in the rainbands contributed the most to the 7 mm h^{-1} peak. The 1–2 mm h^{-1} rainfall mostly occurs between the eyewall and rainbands. The total distribution in Fig. 6 is skewed toward higher rates, which shows that convective-type rainfall from the eyewall and rainband dominates the distribution. The change in the PDF of rain occurrence as a function of the radial distance to the storm center is shown in Fig. 7. Within the inner 50-km radius, the mode sharply increases with distance reaching 10 mm h^{-1} at the 50-km radius. Between 50 and 75 km, the distribution broadens because of the rainfall asymmetry present in Dennis's eyewall (Fig. 4). Between 75 and 200 km, the mode decreases with distance, from approximately 10 mm h^{-1} to 4 mm h^{-1}. The distribution narrows as the storm shows a more

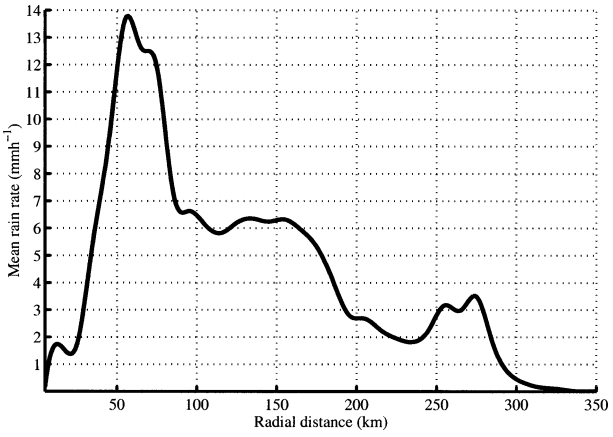

FIG. 5. Radial profile of azimuthally averaged rain rates for Dennis on 28 Aug 1999.

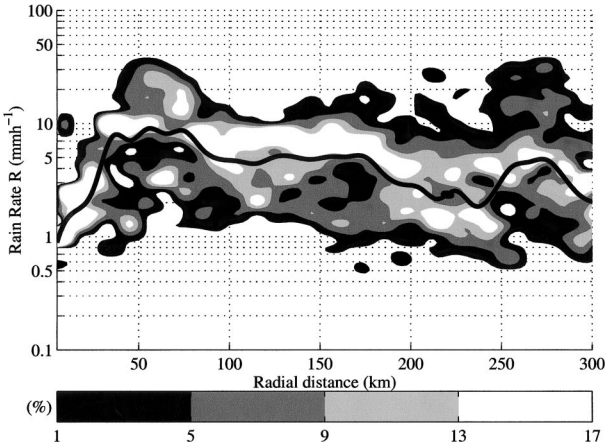

FIG. 7. Radial variation of PDF for Dennis, from the storm center to 300-km radius. The black line shows the median rain rate as a function of the radial distance to Dennis's center.

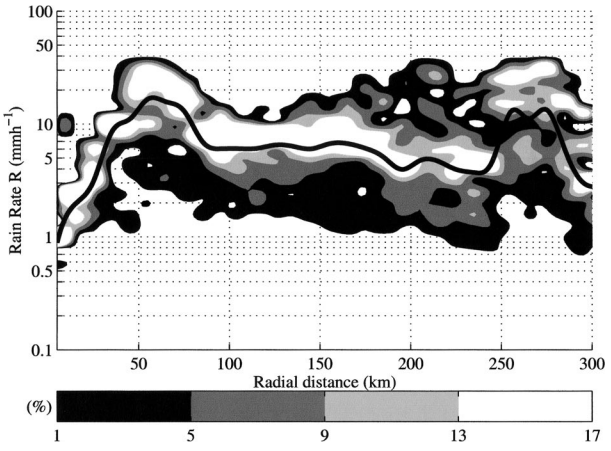

FIG. 8. Same as in Fig. 7 except for the rainfall flux, defined as the rainfall multiplied by the area that it affects.

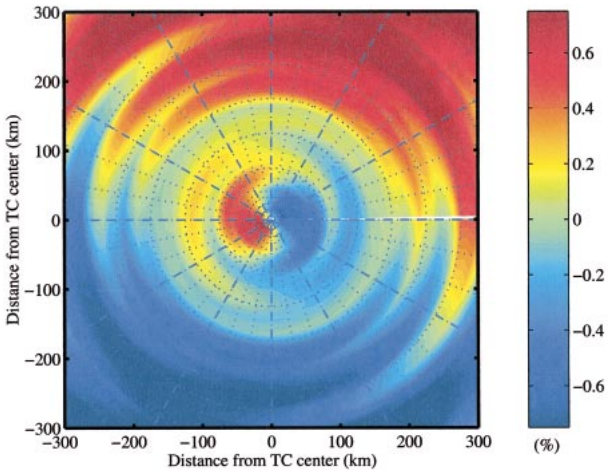

FIG. 9. Normalized phase maximum of the first-order rainfall asymmetry in Hurricane Dennis, as a function of the distance from the storm center. The first-order Fourier coefficients are calculated relative to the storm motion direction.

horizontally uniform rain pattern. Further out, the distribution broadens again and the mode increases, due to the presence of the right-front rainband. In general, the width of the PDF provides good indications of the degree of symmetry of the storm rainfall. Dennis's PDF illustrates that even at large distances (>300 km), high rainfall rates (>40 mm h^{-1}) can be observed, although the probability is only a few percent.

Figure 8 shows the rainfall flux PDF with radial distance for Hurricane Dennis. Compared to the PDF of rain occurrence (Fig. 7), both the mode and median of the distribution in Fig. 8 occur at higher rain rates, although differences between the modes of both figures are small. The rainfall flux distribution is heavily influenced by large rates, which is shown by the large shift in the median from the PDF of occurrence to the rainfall flux PDF. The shift toward higher rates is more pronounced for the median than for the mode, particularly in the eyewall and rainband areas. In these two areas, most of the rain flux can be attributed to rainfall rates >3–4 mm h^{-1}. Those two regions are also the areas with the largest asymmetries, where rates >20 mm h^{-1} were observed. The medians for both distributions are very similar in the region between 75 and 250 km, where the storm was more symmetric.

To examine the asymmetry in the spatial distribution of rainfall, the first-order Fourier analysis of Dennis rainfall is computed relative to the storm motion, using Eqs. (2)–(4). The solid dots on top of the rainfall map in Fig. 4 show the general location of the first-order asymmetry phase maximum. The three dots corresponding to the inner 150-km radii are located primarily on the left of the storm center, in agreement with the asymmetry in the eyewall rainfall. The three dots corresponding to the radii between 150 and 300 km are located in the front-right quadrant, where the rainband precipitation is observed. Figure 9 shows the wavenumber-1 asymmetry spatial distribution within 300 km of Dennis's center. Larger asymmetries are observed at larger radii. Asymmetry amplitudes are much smaller near the center, as the rainfall surrounds the entire storm eye. The amplitudes in Fig. 9 are normalized to the ambient mean rainfall, so that the amplitude near unity ahead of the center at 275 km means that the wavenumber-1 signal is as strong as the axisymmetric average. The various analyses introduced in this example are applied to the extended 3-yr statistics in the next section.

4. Characteristics of the TC rainfall distribution

a. PDF of rain rates

Figure 10 shows the PDF distributions by area of occurrence for all TRMM rainfall observations within an area of 500-km radius around the storm center. The mode is near 1 mm h^{-1}, but not unique, as all distributions in Fig. 10 show a second maximum near 3.2 mm h^{-1}. As the storm intensity increases, the median and the mode of the distribution shift toward higher values and the distribution tends to become broader (Fig. 10b).

Similar characteristics are observed in the basin PDFs (Fig. 10c). The Atlantic basin distribution is similar to the overall PDF for CAT12 and CAT35, which is not surprising as more observations of hurricanes were obtained in the Atlantic than in other basins during the 1998 to 2000 period (Table 1). ECPAC has the least total rain of all basins with a narrower distribution and one of the largest percentage of TS observations (Table 1). In agreement with the results of Fig. 10b, ATL and ECPAC define the envelope for the remaining basin PDFs. However, the trend in the remaining basins is not as clear, as illustrated by the NIND, SIND, and SPAC PDFs. Those three basins show some differences in the modal frequency and amplitude of the PDF, although distributions among intensities are similar for each basin

(Table 1). Hence, the TC intensity is most likely not the most important factor explaining the PDF distribution by occurrence between basins.

b. Azimuthal averages

The radial distributions of azimuthally averaged rainfall rates for all observations and each of the three storm intensity categories are shown in Fig. 11a. Rain rates up to 5 mm h^{-1} are found within 50 km of the TC center for all observations. They decrease outward to 1 mm h^{-1} at 250 km. The maximum rain rate is located at 40 km from the storm center. Mean rain rates increase with storm intensity at all radii. Peak mean rates are 3, 7, and 12.5 mm h^{-1} for TS, CAT12, and CAT35 systems, respectively. The location of the peak rainfall also varies with intensity, from about 50 km from the storm center for TS to 35 km for CAT35 systems. Marks (1985), using a rainfall distribution from airborne radar observations for Hurricane Allen (1980), showed a mean rain rate of 11.3 mm h^{-1} in the eyewall and 1.8 mm h^{-1} in the region extending from the outer edge of the eyewall to a radius of 111 km. At the time of the measurements, Allen's minimum sea level pressure (SLP) varied from 960 to 910 mb, making it an upper CAT12 to CAT35 in our description. The radius of maximum wind in Allen fluctuated between 12 and 40 km. Assuming that the peak rain rates in the TRMM distribution can be identified with the mean location of the eyewall, the peak rates observed with TRMM for CAT12 to CAT35 storms compare well with Marks's (1985) findings.

In the TRMM statistics, the area extending from the eyewall (35–40 km) to the 111-km radius yields 8.4 and 5.7 mm h^{-1} for CAT12 and CAT35 storms, respectively. These rates are larger than those mentioned in Marks (1985). However, TRMM probably overestimates the rain rates in the central dense cloud overcast (CDO) region (Lonfat et al. 2000). Rain rates in Allen also decreased more sharply with radius compared to other observations by Burpee and Black (1989). These authors also partitioned the observations into the eyewall and rainband regions. Hurricane Alicia's eyewall fluctuated between 20 and 35 km, while Hurricane Elena's eyewall remained at 35 km. The rainband region in Burpee and Black (1989) extended to 75 km, instead of the 111 km as in Marks's study. Both storms were classified as CAT12, with minimum SLP near 960 mb. Rain rates of 5.2 and 6 mm h^{-1} in the eyewall and 2.8 and 3.4 mm h^{-1} in the rainband were observed in Alicia and Elena, respectively. TRMM CAT12 mean rates in the eyewall and in the region extending from 35 km to 75 km were 7 and 6.4 mm h^{-1}, respectively. The ratio of eyewall to rainband rain rate was near 1.8 for both Alicia and Elena. The same ratio calculated with TRMM was 1.1. Hence, the TRMM rates in the rainband region are high compared to that from the radar studies.

Miller (1958) provides a comparison of rainfall in the outer region. The inner 1° box (~60 km radius) and the average of the 8 surrounding 1° boxes (~200 km radius) yield 6.6 and 3.2 mm h^{-1} for the inner and outer regions, respectively. Using the TRMM CAT12 distribution with 60- and 200-km radii, the means are 6.7 and 3.9 mm h^{-1}, respectively. Including a larger area in the rainband mean calculation provides a better result, confirming that TRMM tends to overestimate the rain in the region outside the eyewall.

Differences in the mean rain rates of various TC intensities occur almost exclusively within 250 to 300 km

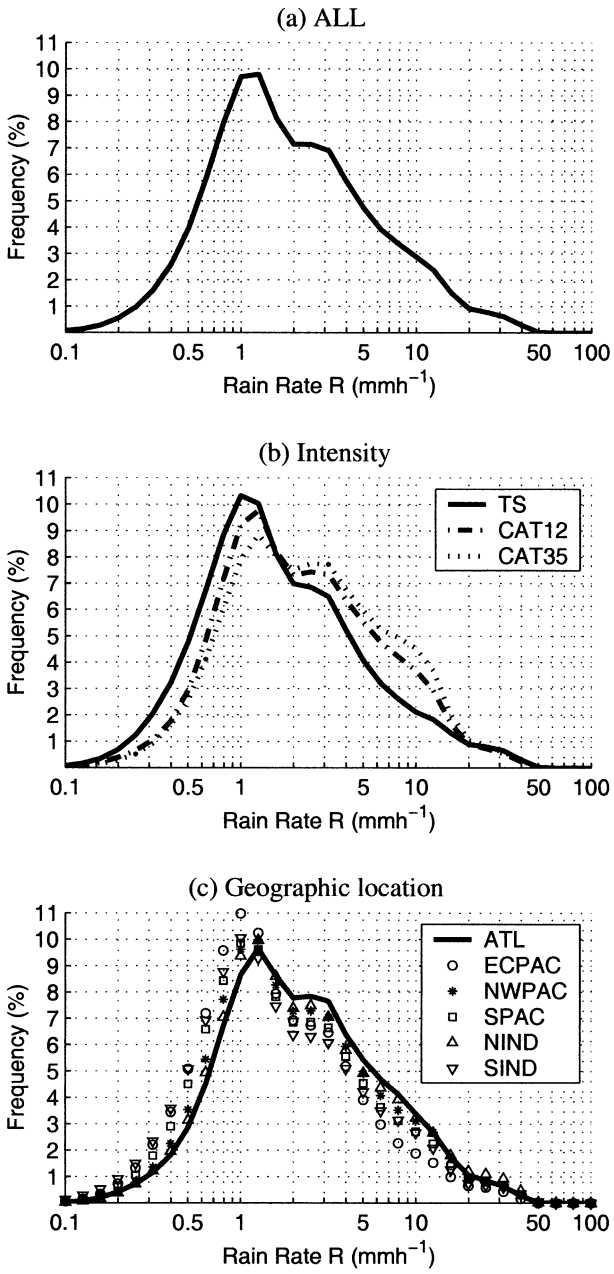

FIG. 10. Probability density functions calculated within 500-km radius of storm center (a) for all 2121 observations, (b) for TC intensity groups, and (c) for oceanic basin subgroups.

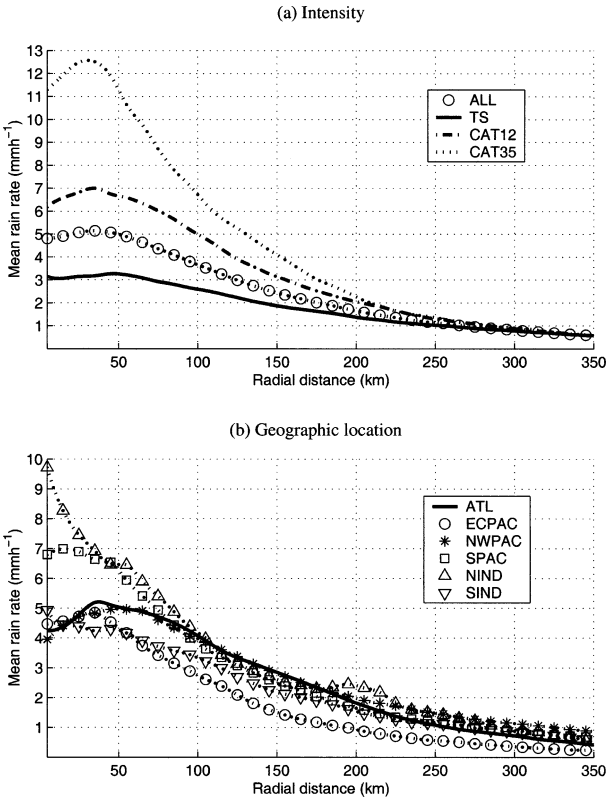

FIG. 11. Mean rain rates, all 2121 1998–2000 observations, (a) as a function of storm intensity, and (b) as a function of geographic locations.

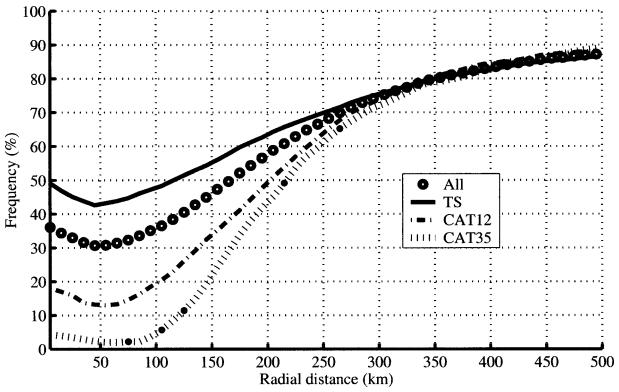

FIG. 12. Radial distribution of nonraining observations stratified by TC intensity.

of the storm center, which is partly associated with the different relative contribution of convective to stratiform precipitation at various intensities (Lonfat et al. 2000). Furthermore, the frequency distribution of nonraining area with radius relative to the total area also contribute to the variability (Fig. 12). Less than 5% of all observations are larger than 15 mm h^{-1} at 250-km radius, which is true for all storm intensity groups (Fig. 13). The nonraining area in Fig. 12 reaches 65% of the entire area within 250 km. The distributions of nonraining area with TC intensity merge by the 300-km radius. The decrease in heavy rain, combined with a sharp increase in nonraining area, most likely explains the variability in the mean rainfall within 250 km of the center.

Figure 11b shows the azimuthal mean rain rates stratified by TC geographic location. The variability in mean rainfall is large from basin to basin. The mean rain rates vary between 4 and 10 mm h^{-1} within the inner 50-km radius. The NIND basin TCs show larger rates than the other basins within the inner 100-km radius. Although the remaining basin distributions look similar, up to 50% differences in mean rates between basins are observed within the inner 250 to 300 km. The ECPAC TCs rain less than other basins throughout most of the 350-km radius shown in Fig. 11b. Three possible scenarios may explain the basin variability: (a) biases in the TC intensity sampling may artificially increase or decrease the true basin averages by altering the distribution of observations among the different TC intensity classes in each basin; (b) the TC variability among intensity classes in each basin may be responsible for the different basin distributions; and (c) differences in the TC-environment interactions in each basin may alter the distribution associated with intensity changes shown in Fig. 11a.

Our results do not support the first two scenarios. The variability observed in Fig. 11b cannot be explained by a sampling problem. The TRMM observation distribution is representative of the natural global distribution of TCs, as expressed by the best track information in Table 1. The ATL basin showed more similar mean rain estimates than other basins, such as NWPAC, even though it had more observations of CAT12 and CAT35 than any other basin between 1998 and 2000. Also, the two basins showing the largest rainfall rates (NIND and SPAC) have only 36% and 31% of observations in the hurricane categories, respectively. ECPAC and NWPAC have similar frequencies, although their mean R distributions in Fig. 11b show smaller rates throughout the radial distribution. Consequently, the intensity trend shown in Fig. 11a does not apply to all basins. Hence, the way intensity and rainfall correlate in each basin must depend on the state of the environment and ocean–atmosphere boundary layers, suggesting (c) is most likely the scenario. The intensity trends in each basin need to be computed to confirm this assumption. However, the current database, described in Table 1, is not large enough to provide significant results in all basins for CAT12 and CAT35.

c. Rain-rate probability with radial distance

Figures 13 and 14 show how the CFRDs by area of occurrence evolve with radial distance to the TC center. The CFRDs are computed outward to the 500-km radius from the TC center. Figure 13 shows the CFRD by area

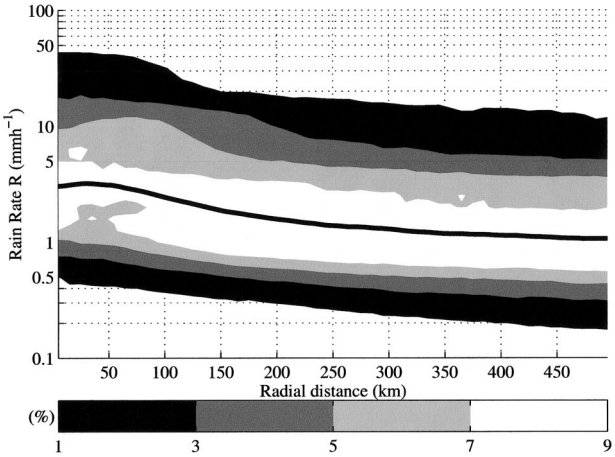

FIG. 13. Radial distribution of rainfall PDF computed for 2121 observations. The color scale refers to the frequency of occurrence of rain rates (in dBR scale) at any radial distance from the center. The black line shows the azimuthal mean rainfall with radial distance.

for all 2121 observations. The mode decreases from 4 mm h^{-1} in the inner 50 km to 1 mm h^{-1} by the 200-km radius. At ranges >200 km, the peak remains at 1 mm h^{-1}.

An important property of the TC rainfall distribution that the PDF does not account for is the frequency of occurrence of nonraining observations. The nonraining area is expected to increase with radial distance, as the area itself increases with the square of the radius. The circled curve in Fig. 12 shows the radial distribution of nonraining observations. The values are the frequencies of zero rain observations relative to the total number of observations at any distance from the TC center. Inferring that those values represent the storm nonraining area assumes that our sampling of rain and no-rain areas is uniform, as TRMM does not observe the entire storm area. This assumption is most likely legitimate, as the total number of TRMM observations obtained in each quadrant of the storm is similar.

Several interesting features are noticeable in Fig. 12. The nonraining frequency increases with distance outward of 50–100-km radius. A frequency minimum is observed near 50-km radius (typical radius of maximum rain). Frequencies increase in the inner 30 to 50 km. The inner 50-km increase in frequencies indicates the presence of the eye. The frequency minimum corresponds to the mean location of the eyewall, and the trend of increasing frequencies with radial distance corresponds to the increase in area that is not matched by the rainfall contribution as the radius increases.

Figure 14 shows the CFRD distributions by area, grouped by storm intensity. The distributions vary with intensity within the 250–300-km radius of the storm center. In that region, the mode increases with intensity. Tropical storms have a broader distribution than CAT12 and CAT35 in the inner 250 km. Assuming that the width of the distribution is a measure of the asymmetric

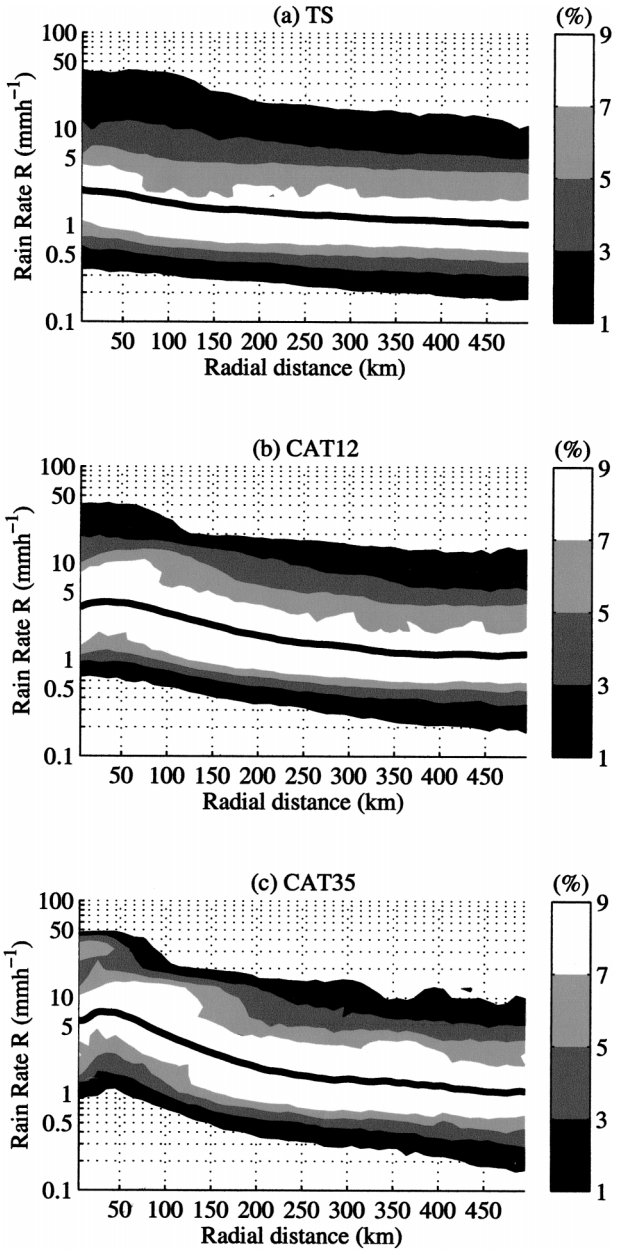

FIG. 14. Radial distribution of rainfall PDFs for (a) TS, (b) CAT12, and (c) CAT35 storms. The color scale and black lines are as described in Fig. 13.

nature of the TCs, TSs seem more asymmetric in the inner core. In the region beyond 250 km, the CFRDs of CAT12 and CAT35 broaden, indicating an increase in the asymmetry amplitude. In the outer area (range > 250 km), the mode is found at 1 mm h^{-1}, uniformly through all PDFs. The CFRDs in Figs. 13 and 14 show that at radii >250 km, for all intensities, rain rates >40 mm h^{-1} can still be observed with a probability of a few percent.

The general features of the no-rain distribution hold true when the data are partitioned with storm intensity.

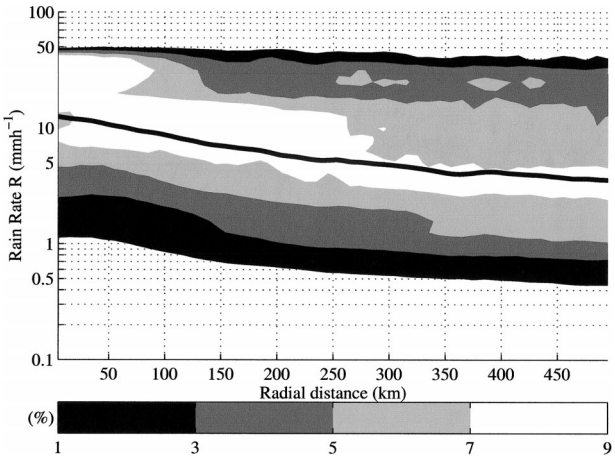

FIG. 15. Same as in Fig. 13 except for the rainfall flux. The rainfall flux is defined as the rainfall rate multiplied by the affected area. Therefore, one 10 mm h^{-1} observation weighs as much as ten 1 mm h^{-1} observations in the PDF of rainfall flux; 1 and 10 mm h^{-1} weigh the same in the PDF of rainfall (Fig. 13).

A strong variability in the no-rain frequencies exists within the inner 350 km of the TC (Fig. 12). Nearly half of all observations in the inner 150 km of TSs are nonraining, while 90% of observations correspond to rain in the same area for CAT35. The inner 150-km region of CAT12 shows 20%–30% nonraining area. There is a distinct change in distributions from TS to CAT12 and CAT35. This change is most likely associated with the dynamic structure of the storm. As the intensity increases, the transport of rainfall by the swirling winds may more efficiently redistribute the rainfall around the entire storm. Rain that may be produced locally in convective cores is going to spread over greater areas as the wind increases (e.g., Marks and Houze 1987). The number of convective cores may increase in the stronger systems. At large radii, the distributions of nonraining observations as a function of intensity all merge and the nonraining area does not increase geometrically, which means that the area where rainfall occurs increases with radial distance.

The relative contribution of each rain rate to the total volume (flux) of precipitation is shown in Figs. 15 and 16. Figure 15 shows the CFRD of flux for all 2121 TC events. The inner core mode is at 30 mm h^{-1} and extends to the 50-km radius. A second mode, at 11 mm h^{-1}, extends from 40 to about 240 km. At large distances, the mode shifts toward 3 mm h^{-1}. The steplike mode structure with radial distance is also observed when the observations are stratified by intensity. The modes are found at similar rain rates at all intensities, but their amplitudes vary with the storm strength. As the storm becomes more intense, the width of the PDF narrows, so that the mode frequency increases. This trend holds particularly well within the inner 300 km. At further distances, the PDFs look very similar, taking into account that the size of the dataset reduces with TC intensity, which introduces some noise in the PDF. While the high rain rates (>10 mm h^{-1}) make up $<15\%$ of the total inner core area, for all 2121 observations averaged together, they contribute about 50% of the total rainfall. Similarly, Marks (1985) found that the eyewall rainfall in Allen contributed to nearly 40% of the total amount within a radius of 1° latitude from the storm center. All TMI distributions have an upper limit near 50 mm h^{-1}. These higher rates contribute less than 1% to the total volume of rainfall within the storm.

d. Rainfall asymmetry

Figure 17 shows the storm-motion-relative spatial distribution of rainfall asymmetry for all observations globally (Fig. 17a) and for each intensity group (Figs. 17b–d), respectively. The overall storm composite shows that M_1 maximum is located in the front quadrants (Fig. 17a). This asymmetry is similar for TS (Fig. 17b). However, as the storm intensity increases, the M_1 maximum shifts from the front-left to the front-right quadrant. The shift suggests that the rainfall asymmetry correlates with the asymmetry in the tangential wind circulation.

The asymmetries in CAT12 and CAT35 storms are consistent with those observed by Burpee and Black (1989) and Marks (1985). Burpee and Black observed a strong wavenumber 1 in the composite rainfall structure of Hurricane Alicia. The maximum rainfall was observed in the front-left quadrant and the minimum in the rear-right quadrant, for both the eyewall and the rainband area within 75-km radius. In the eyewall, the maximum was 2.5 times larger than the minimum. In Elena, Burpee and Black observed a rainfall maximum in the front-right of the storm center. Elena had a stronger rainfall asymmetry than Alicia, with a maximum-to-minimum ratio of 7. Marks found a front-right maximum rainfall in the eyewall region of Hurricane Allen. These features are similar to the observed patterns in Figs. 17c,d. As the storm evolves, the asymmetry varied substantially. Burpee and Black noted a large variability in the asymmetry of Hurricane Alicia. However, coastal influences may explain some of the variability in their observations.

The differences in asymmetry amplitude among the various intensity groups are likely related to the strength of the primary circulation of the vortex. Tropical storms have the largest asymmetry throughout the 300-km area. The amplitudes reach 30% of the azimuthal mean rainfall at 300 km in the front of the storm center. Although TSs have a weaker and less organized circulation than CAT12 and CAT35 storms, deep convection does not seem to be randomly distributed around the storm center. Most TSs are aggregates of mesoscale convective systems in the early stage of their life cycle. The rainfall maximum is in the front of the storm center (Fig. 17b), where the friction-induced asymmetry in the circulation of the moving storm may play an important role in

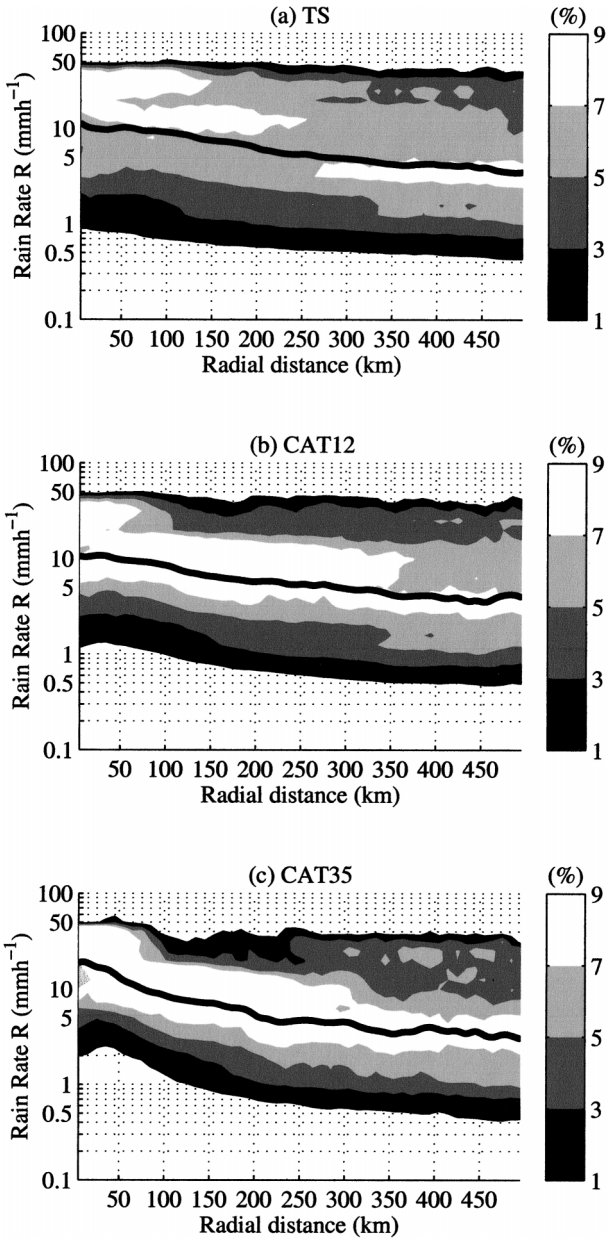

FIG. 16. Same as in Fig. 14 except for the rainfall fluxes.

enhancing the deep convective activity by creating a low-level convergence anomaly ahead of the storm. As the storm intensity increases, the primary circulation becomes stronger and more symmetric (e.g., Marks and Houze 1987; Croxford and Barnes 2002) (Fig. 17d). This simple picture does not take into account the various possible physical processes that may affect the TC rainfall asymmetry, as will be discussed in the next section.

Figure 18 shows the TC rainfall asymmetry as a function of the geographic locations. In all basins, the M_1 maximum is located in the front quadrants. However, large differences in rainfall asymmetry are also evident among different basins. There are significant differences between the Northern and Southern Hemisphere asymmetry distributions. The TCs in the Southern Hemisphere have a clear M_1 maximum in the front-left quadrant (Figs. 18d,f). In the Northern Hemisphere, M_1 peaks in the front-right quadrant. This is particularly evident in the Atlantic basin (Fig. 18a). It is interesting that M_1 maximum shifts cyclonically from the center outward in both ECPAC and NIND (Figs. 18b,e), whereas it is shifted anticyclonically and much weaker in the NWPAC. The M_1 maximum in Atlantic TCs remains in the front-right quadrant from the center out to 300 km, which is in agreement with the location of maximum lightning occurrence in Atlantic hurricanes found by Corbosiero and Molinari (2003). The first-order asymmetry amplitudes increase outward from the center in all basins. The TCs in NWPAC and SPAC basins (Figs. 18c,d) have the smallest asymmetry, whereas the Indian Ocean TCs (Figs. 18e,f) have the largest.

5. Factors affecting rainfall asymmetry

Several factors are known to affect TC rainfall asymmetry, such as advection of planetary vorticity, vertical wind shear (e.g., Rogers et al. 2003), and friction-induced convergence in the boundary layer (e.g., Marks 1985). The differences in rainfall asymmetry observed between the Northern and Southern Hemispheres (Fig. 18) seem to indicate advection of planetary vorticity plays a critical role, particularly in weak TCs. The amplitude of rainfall asymmetry is small in hurricanes (less than 15% of the ambient mean rain amount within the inner 300 km). The distinct patterns of rainfall asymmetry for different ocean basins (Fig. 18) seem to indicate both the friction induced low-level convergence and vertical wind shear must play a role as well. However, it is difficult to examine the complex effects of vertical wind shear without a good global wind dataset. Hence, the following discussion focuses on the effects of boundary layer convergence on the observed rainfall asymmetry.

The importance of the TC motion on rainfall asymmetries is investigated by dividing the dataset into two groups: fast- (>5 m s^{-1}) and slow- (<5 m s^{-1}) moving TCs. Figure 19 shows the spatial distribution of M_1 for the two groups. There is no significant difference in M_1 pattern for the slow- and fast-moving TCs, except the amplitude is larger for the fast-moving TCs. The M_1 maximum is ahead of the storm center for both groups, consistent with the overall TC asymmetry shown in Fig. 17a. However, the amplitude of M_1 varies with the speed of the storms at large radii (Fig. 19). At 275 km from the storm center, faster TCs have amplitudes as large as 50% of the ambient mean rain rate, while the amplitudes for the slower TCs do not reach 20% of the ambient value. Shapiro (1983) studied the effect of the storm motion on the boundary layer of a hurricane inner core (within approximately 50-km radius). A convergence

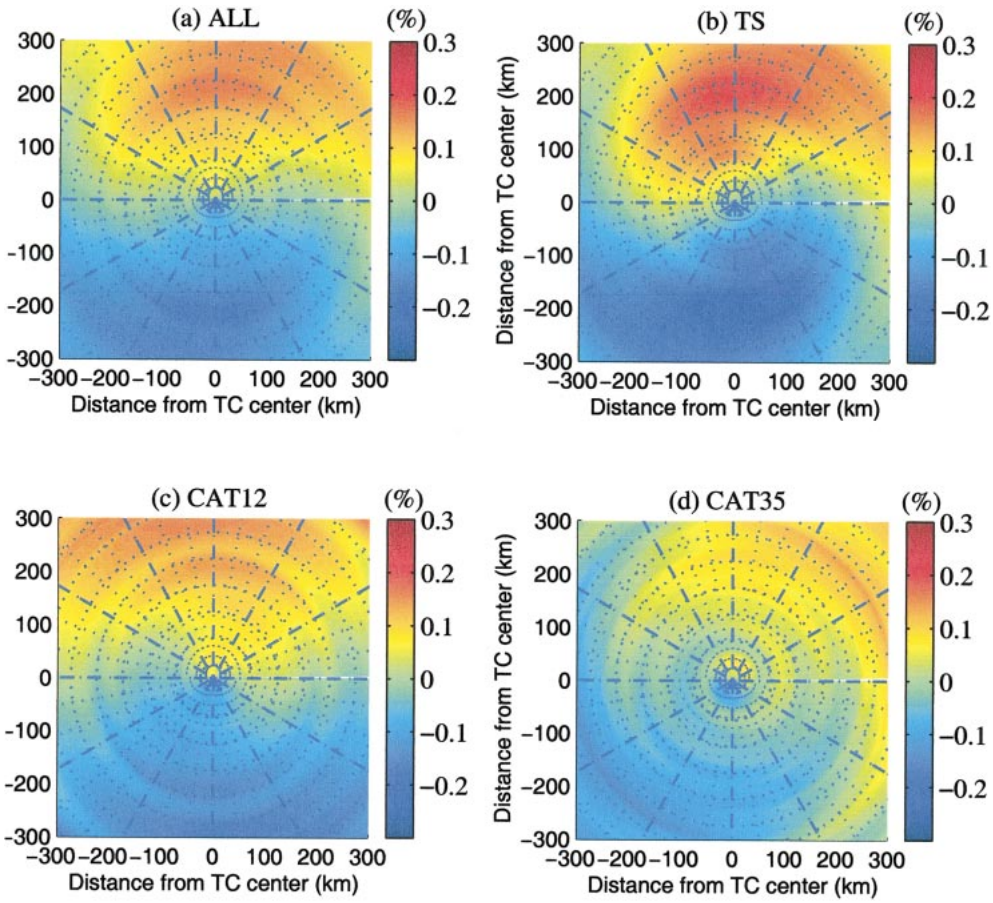

FIG. 17. Rainfall asymmetry calculated in 10-km rings around the storm center, as a function of storm intensity: (a) 2121 TC observations (total distribution), (b) TS, (c) CAT12, (d) CAT35. The storm motion vector is aligned with the positive *y* axis. The color scale indicates the amplitude of the normalized asymmetry. The red corresponds to the maximum positive anomaly and the blue the minimum rainfall within the storm.

anomaly was observed in front of the storm, resulting in enhanced rainfall ahead of the storm center. The anomaly shifted from the front to the front-right quadrant with increasing storm speed. Hurricanes Alicia and Elena (Burpee and Black 1989) were slow movers. Alicia's speed increased from 1.5 to 2.3 m s^{-1} during the period of observation. The maximum rainfall shifted from the left to slightly right of the track with increasing speed. The asymmetry amplitude remained similar. Hurricane Elena, slightly faster at 5 m s^{-1}, had maximum rainfall in the front-right quadrant. However, the asymmetry amplitude in Elena was twice as large as in Alicia. Although Hurricane Allen was moving much faster than Alicia and Elena, at 10 m s^{-1}, its asymmetry location and amplitude were comparable to that in Elena. This complexity is closely related to the storm environmental conditions as well as storm–environment interactions, which are not well understood.

Each intensity and oceanic basin group can be further divided into the two speed categories defined previously. The number of TCs with translation speed <5 m s^{-1} is about 60% for TS, 48.5% for CAT12, and 56.6% for CAT35, respectively. These numbers do not vary much with storm intensity, although CAT12 storms are slower on average than other groups. However, the TC translation speed varies significantly from basin to basin. Of ATL storms, 43% were slow movers, compared to 50.5% in ECPAC, 56% in NWPAC, 76.8% in NIND, 74.9% in SPAC, and 60.8% in SIND systems. Tropical cyclones in the Indian Ocean basins and the South Pacific are slow movers, while the Atlantic storms are the fastest on average. If the variability in translation speed can explain the rainfall asymmetry, one would expect the Atlantic storms to show the largest asymmetry amplitudes, while the Indian Ocean and South Pacific storms should be more symmetric. Results shown in Fig. 18 do not confirm this. Hence, other mechanisms, such as the vertical wind shear must play at least as important a role as the translation speed on TC rainfall distributions.

6. Conclusions

Precipitation distributions in TCs have been studied globally using observations from the TRMM/TMI. Be-

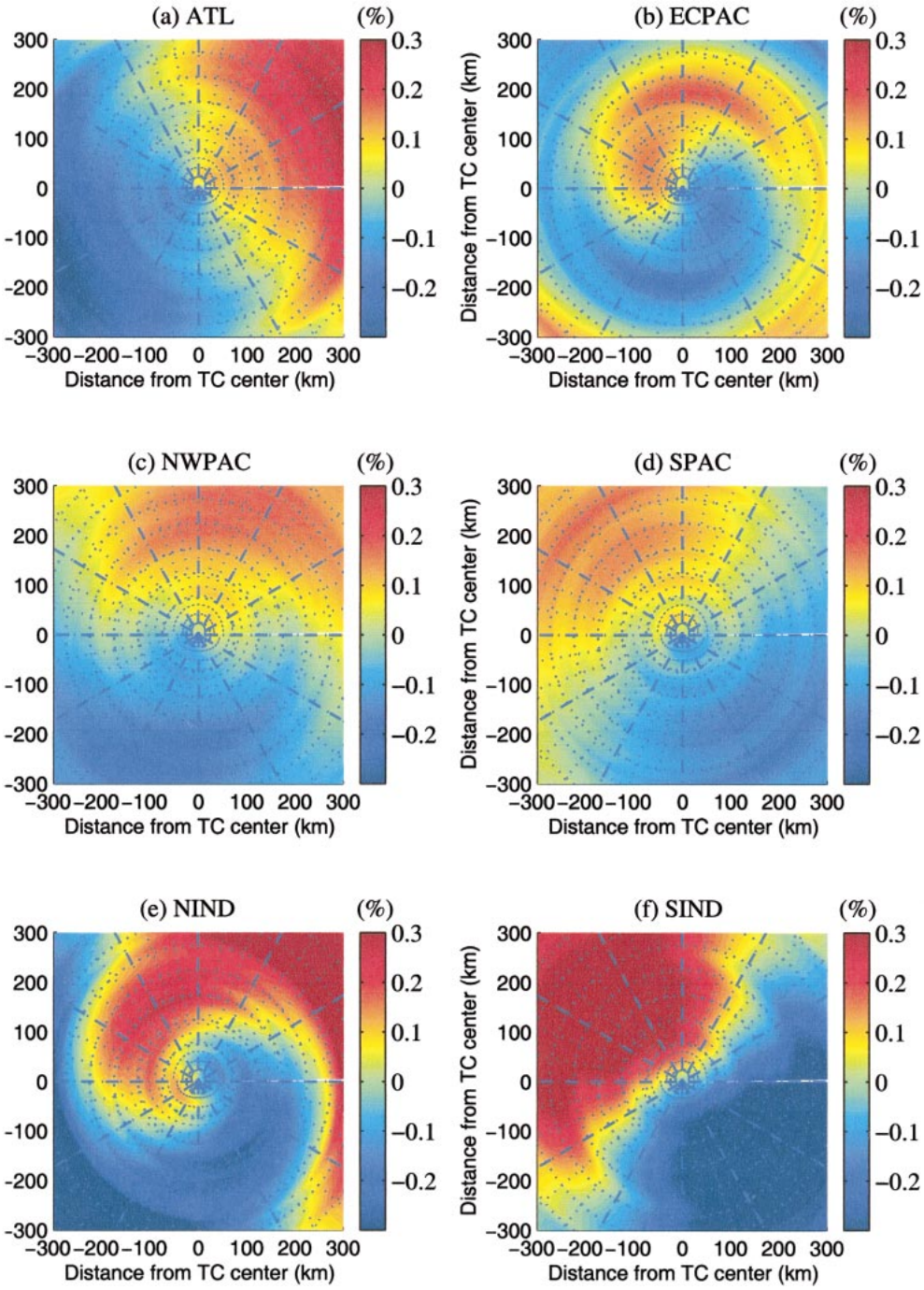

FIG. 18. Rainfall asymmetry for the six oceanic basins: (a) ATL, (b) ECPAC, (c) NWPAC, (d) SPAC, (e) NIND, and (f) SIND.

tween 1 January 1998 and 31 December 2000, 2121 instantaneous measurements were collected in 260 TCs with intensity ranging from tropical storm to category 5 hurricane in all oceanic basins. The spatial distribution of rainfall is partitioned into an azimuthal average and a wavenumber-1 asymmetry. PDFs are constructed as a function of TC intensity and geographic location.

The PDF analysis is used for comparison of TRMM distributions with previous studies. TRMM/TMI PDF captures the general features described by previous studies. TMI underestimates the small rates (<0.25 mm h^{-1}), which is probably due to the instrument resolution. The frequency for rain rates <2.5 mm h^{-1} is too high, which indicates that the TMI algorithm may redistribute the

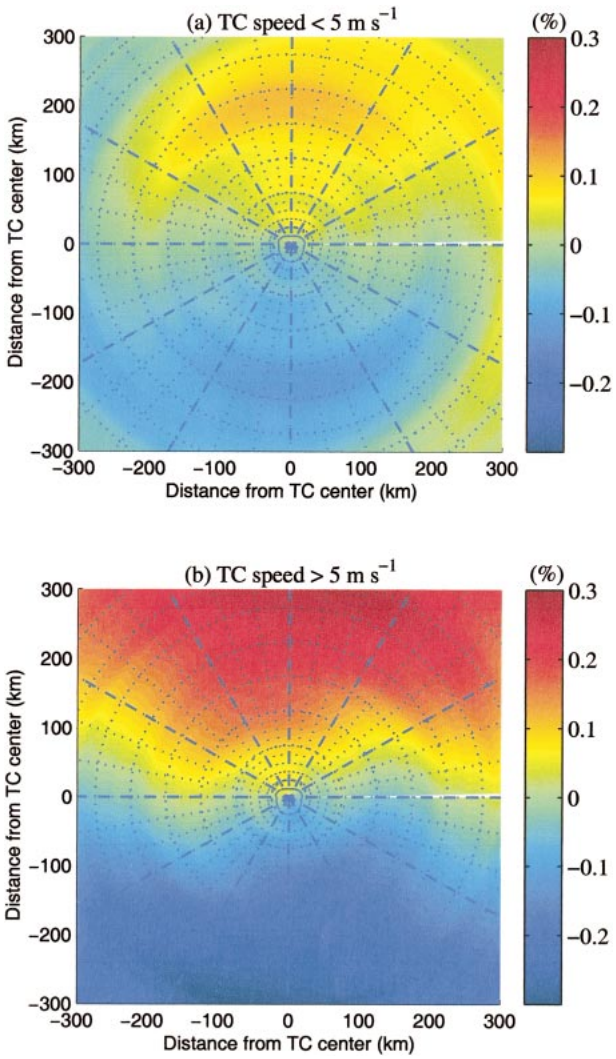

FIG. 19. Rainfall asymmetry as a function of the storm translation speed: (a) $v < 5$ m s^{-1}, and (b) $v > 5$ m s^{-1}.

lowest rates to the adjacent rainfall bins. This problem does not bias our analysis, except in a region extending between 100 and 250 km, where the 1 to 2.5 mm h^{-1} rates are most prevalent. The asymmetry analysis is independent of the absolute values of the estimates, because the quadrant rates are normalized to the ambient azimuthal mean rates. The maximum rate observed by TMI is ~50 mm h^{-1}, with a frequency of ~1%. More generally, the heavy rainfall ($R > 10$ mm h^{-1}) covers only 15% of the inner core area, but contributes 50% of the total rainfall amount.

The location of the peak azimuthal mean rain rate shifts to a smaller radius when the TC intensity increases, similar to the observation of Rodgers and Adler (1981) and Marks (1985). The Indian Ocean storms show the largest azimuthal mean rain rates of all basins. Atlantic and west Pacific storms have very similar mean distributions. East-central Pacific storms show the smallest mean rates, possibly because of the cooler SST conditions prevailing in the eastern Pacific region. However, the intensity relationship deduced for the total database does not apply in each basin. Consequently, how the storm intensity and the rainfall distribution relate to each other depends on the environmental conditions, specific to each basin.

The wavenumber-1 asymmetry in TC rainfall is found to shift from the front-left to the front-right quadrant with increasing intensity. The tropical storms show the largest asymmetry. Hurricane-strength storms tend to have a more axisymmetric inner core. In all basins, the asymmetry remains in the front quadrants. The storm location is an important factor, as Southern Hemisphere storms show asymmetry to the left of the storm track, while Northern Hemisphere cyclones rainfall peaks in the front-right quadrant. The storm translation speed also plays an important role in the rainfall asymmetries. The rainfall maximum is located in front of the storm center at all speeds, but its amplitude increases with speed. Consequently, frictional convergence, as mentioned by Shapiro (1983), most likely plays an important role on the rainfall structure. However, the basin-to-basin variability in storm motion alone cannot explain the rainfall asymmetry. Hence, other mechanisms, such as the vertical shear may play an important role in the rainfall distributions.

The next step in the analysis will be to study the asymmetries in a shear-relative coordinate system, instead of in the motion-relative coordinate system. Rogers et al. (2003) derived a relationship between the track-relative location of the accumulated rainfall and the direction of the vertical shear vector relative to the storm direction using the fifth-generation Pennsylvania State University–National Center for Atmospheric Research Mesoscale Model (MM5) simulations of Hurricane Bonnie. The total precipitation showed strong sensitivity to the shear direction and amplitude. The rainfall was found to accumulate down-shear left, so that depending on the direction of motion, relative to the orientation of the shear, the spatial distribution of total rainfall along the track could be either symmetric or strongly asymmetric. TRMM, alongside global wind data, can provide statistical information regarding the effect of shear on the instantaneous precipitation distribution. However, the relative contribution of the shear effect with respect to other processes such as frictional convergence or the β-effect mechanism is still not clear. Using TRMM, a detailed diagnostic study of the relative contribution of all processes can be constructed globally. Numerial simulations, along with the results described here, will allow improvements of our knowledge of the precipitation structure of tropical cyclones and of the dynamics governing the rainfall structure. The results from this study can be used as a climatologic basis toward improving the current forecasting techniques. The mean TC rainfall distribution can help correct simple rules of thumb, still a common practice today. Including the asymmetry

analysis will further refine current techniques, as most often the precipitation structure shows at least some degree of asymmetry.

Acknowledgments. We thank Jeffrey Hawkins and two anonymous reviewers from their helpful comments and suggestions. The first author is supported by the NASA Earth Science System Fellowship (NGT5-30425). This work is partially supported by a NASA Grant NAG5-10963 and a NSF Grant ATM9908944.

REFERENCES

Boyd, J. P., 2001: *Chebyshev and Fourier Spectral Methods.* 2d ed. Dover, 44 pp.

Burpee, R. W., and M. L. Black, 1989: Temporal and spatial variations of rainfall near the centers of two tropical cyclones. *Mon. Wea. Rev.,* **117,** 2204–2218.

Corbosiero, K. L., and J. Molinari, 2003: The relationship between storm motion, vertical wind shear, and convective asymmetries in tropical cyclones. *J. Atmos. Sci.,* **60,** 366–376.

Croxford, M., and G. M. Barnes, 2002: Inner core strength of Atlantic tropical cyclones. *Mon. Wea. Rev.,* **130,** 127–139.

Frank, W. M., 1977: The structure and energetics of the tropical cyclone. Part I: Storm structure. *Mon. Wea. Rev.,* **105,** 1119–1135.

Gray, W. M., 1984: Atlantic seasonal hurricane frequency. Part I: El Niño and 30 mb quasibiennial oscillation influences. *Mon. Wea. Rev.,* **112,** 1649–1668.

Jordan, C. L., D. A. Hurt, and C. A. Lowrey, 1960: On the structure of hurricane Daisy on 27 August 1958. *J. Meteor.,* **17,** 337–348.

Kessler, E., 1958: Eye region of Hurricane Edna, 1954. *J. Meteor.,* **15,** 264–270.

Kummerow, C., W. S. Olson, and L. Giglio, 1996: A simplified scheme for obtaining precipitation and vertical hydrometeor profiles from passive microwave sensors. *IEEE Trans. Geosci. Remote Sens.,* **34,** 1213–1232.

——, W. Barnes, T. Kozu, J. Shiue, and J. Simpson, 1998: The tropical rainfall measuring mission (TRMM) sensor package. *J. Atmos. Oceanic Technol.,* **15,** 809–817.

Lonfat, M., F. D. Marks Jr., and S. S. Chen, 2000: Comparison of TRMM, TMI-PR, and airborne radar data for four major Atlantic hurricanes. *Eos, Trans. Amer. Geophys. Union,* **81** (Fall Meeting Suppl.), Abstract A21G-08.

Marks, F. D., Jr., 1985: Evolution of the structure of precipitation in Hurricane Allen (1980). *Mon. Wea. Rev.,* **113,** 909–930.

——, and R. A. Houze Jr., 1987: Inner core structure of Hurricane Alicia from airborne Doppler radar observations. *J. Atmos. Sci.,* **44,** 1296–1317.

Miller, B. I., 1958: Rainfall rates in Florida hurricanes. *Mon. Wea. Rev.,* **86,** 258–264.

Rappaport, E. N., 2000: Loss of life in the United States associated with recent Atlantic tropical cyclones. *Bull. Amer. Meteor. Soc.,* **81,** 2065–2074.

Rodgers, E. B., and R. F. Adler, 1981: Tropical cyclone rainfall characteristics as determined from a satellite passive microwave radiometer. *Mon. Wea. Rev.,* **109,** 506–521.

——, S. Chang, and H. F. Pierce, 1994: A satellite observational and numerical study of precipitation characteristics in western North Atlantic tropical cyclones. *J. Appl. Meteor.,* **33,** 129–139.

Rogers, R., S. S. Chen, J. Tenerelli, and H. Willoughby, 2003: A numerical study of the impact of vertical shear on the distribution of rainfall in Hurricane Bonnie (1998). *Mon. Wea. Rev.,* **131,** 1577–1599.

Shapiro, L. J., 1983: The asymmetric boundary layer flow under a translating hurricane. *J. Atmos. Sci.,* **40,** 1984–1998.

——, 1987: Month-to-month variability of the Atlantic tropical circulation and its relationship to tropical storm formation. *Mon. Wea. Rev.,* **115,** 2598–2614.

Simpson, J., R. F. Adler, and G. R. North, 1988: Proposed tropical rainfall measuring mission (TRMM) satellite. *Bull. Amer. Meteor. Soc.,* **69,** 278–295.

Wexler, H., 1947: Structure of hurricanes as determined by radar. *Ann. N. Y. Acad. Sci.,* **48,** 821–844.